3D Printing Habitats on Mars Using Martian Regolith Simulant

Reza Hedayati*, Victoria Stulova

Department of Aerospace Structures and Materials, Faculty of Aerospace Engineering, Delft University of Technology (TU Delft), Kluyverweg 1, 2629 HS Delft, the Netherlands

** Corresponding author: rezahedayati@gmail.com*

Abstract

Limitations of manned missions include limited amount of payload that can be transported to the target body, and human vulnerability to harsh pressures, temperatures, and space radiation. Hence, it is preferable that the potential landing location for humans has an already constructed habitat preferably made from in-situ materials. This means that the prospect of utilizing a readily available Martian material, such as regolith, in an easily programmable manufacturing method, such as 3D printing, is very lucrative. The goal of this research is to explore a mixture containing Martian regolith for the purposes of 3D-printing in unfavorable conditions. Regolith has the properties that allow it to act as geopolymer in the presence of appropriate alkaline binder, and hypothetically a very low amount of such binder is needed. For the sake of this research, a simplified binder which consists of water and Sodium Silicate is used. Martian conditions are less favorable for the curing of such mixture because of low temperature and pressure on the surface of the planet. Manufacturing through 3D-printing, as compared to molding, might also have an effect on the resulting mechanical properties. In order to evaluate mechanical properties of the mixture, molding and 3D-printing was conducted at various curing conditions and the results were compared. Due to the combination of low reaction speed at low temperature (2°C) and rapid water evaporation at low pressure (0.1 - 0.01 bar), curing of the specimens at Martian conditions yielded unsatisfactory results. The reaction medium in the form of water was evaporated from the specimen before the curing reaction could progress enough to form a proper geopolymer. Most of such specimens were not robust enough to withstand the beginning of three-point bending test, yet alone to be used as a construction material. The specimens cured at high temperatures (60°C) showed satisfactory results, with highest flexural load achieved up to 9 MPa when cured at 60°C temperature and 1 bar pressure. The specimens manufactured by 3D-printing showed ultimate flexural stress 20% lower than equivalent molded specimens. Overall, the proposed mixture ended up being hardly suitable for the application in very low temperature and pressure conditions, because of its high dependence on elevated temperature and pressure for curing. Exploring potential mixture modifications and performing improved tests using the basis laid in this research might lead to a potentially effective and realistic way of utilizing Martian regolith for unmanned 3D-printing purposes with minimal investment, which is one of necessary goals in making a manned Martian mission possible.

Keywords: Mars; Additive manufacturing; 3D printing; regolith; mechanical properties.

1. Introduction

Since the Apollo 17 mission back in 1972, only highly specialized robots have been sent to other celestial bodies for in-situ exploration, as it is considerably safer and requires little supportive payload. Robots, however, are quite limited in their functionality, as they are used for a particular number of scientific goals, programmed during the robot development [1]. Sending humans instead of robots would provide significantly more flexibility in research and valuable first-hand experience in the location to be explored. However, human lives are considerably more valuable than robots in case of a catastrophic failure and require a lot of equipment in the form of food, water, shelter with all living necessities and space radiation protection at minimum [2]. Due to the latter in particular, the time a human can spend in space environment is very limited [3]. All these basic needs already force the mission to be considerably more expensive as compared to an unmanned one. Hence, to make the most out of manned mission, as much preparation as possible should be done before sending a human to other celestial body [4].

Because of a large sustaining equipment required for a manned mission together with necessary scientific equipment, expected amount of payload to be taken for a manned mission is very high. Therefore, as many in-situ resources as possible have to be utilized for mission cost reduction as well as maintenance convenience [5]. Also, preparing the landing site for astronauts before they arrive can significantly increase the amount of useful research work that can be done in a set period of time, as space radiation limits the amount of time that humans can spend on other celestial bodies. Therefore, 3D-printing can be looked at as a promising manufacturing method for such purpose, as the desired design can be programmed in the printer and simply executed, provided that printing material is supplied [6-10]. If this printing material contains mostly in-situ gathered materials, the amount of necessary payload can be significantly reduced [11].

This research concerns investigating the printing mixtures that can be utilized for Martian 3D printing purposes and selecting the most promising one. This mixture is then tested for overall viability at different manufacturing methods, namely molding and printing, and the conclusion regarding the overall idea is made. As the starting point, Martian regolith simulant is taken as primary material, as the actual Martian

regolith is easy to collect and process from the surface of the planet. The main goal of the research is to find and develop a suitable binder/regolith mixture for Martian regolith 3D printing application, and after a proper investigation make a conclusion about the viability of said mixture. In order to achieve this goal, various specimens were constructed at different conditions, and the properties of the specimens were compared in terms of physical and mechanical properties.

2. Differences between 3D printing on Earth and Mars

Transporting any payload into space is very expensive as compared to transportation costs on Earth. While there is a wide range of materials that can be used for 3D printing on Earth [12-17], only a very limited amount of them can be reasonably transported into space. Transporting large amount of building material to build one or multiple habitats on Mars seems unrealistic, especially considering the fact that the walls of such habitat need to be thick and strong to protect humans from dangerous environmental conditions such as meteoroids and space radiation from which Martian atmosphere offers negligible protection. Hence, it is necessary to use in-situ resources when constructing the habitat, and potentially utilize in-situ resources for synthesis of usable binders. By exploring the underground of the planets, it could be possible to dig and construct an underground shelter, which offers high protection from meteoroid strikes and radiation due to the potentially high wall/ceiling thickness. However, for this to become possible, more exploration is required. If the raw resources are not usable, the possibility of synthesizing a printing material would be open once more information about availability of those resources is better known. This would require extra energy and possibly complex equipment, but the result might make the Martian colony independent from Earth.

As mentioned above, due to near-absence of atmosphere on Mars, small space objects like meteors and asteroids cannot be incinerated by the impact with atmosphere, like it happens around Earth. On Mars, 30,800 kg of meteoroid mass strikes the surface per day [18]. Earth receives considerably less meteoroid mass (between 2,900 and 7,300 kg per year, excluding dust particles), and it is also slowed down considerably by the atmosphere [19]. The danger of meteoroid impact persists not only for potential humans and habitats on Mars, but also for the 3D printing equipment and unfinished habitat. Printing equipment itself can contain vulnerable components which might get damaged

by smaller strikes. Initial stages of printing, which are expected to be most vulnerable due to unfinished sheltering structures and hence exposed printing equipment, are expected to be done without supervising humans, eliminating the possibility of easy repair. Material used for building the habitat should also have enough impact resistance to withstand small strikes.

Unlike on Earth, where the presence of atmosphere and water stabilizes the temperature in each region, Mars has large temperature fluctuations during the day/night cycles. Martian surface experiences a swing from $-153°$ to $+20°$ near the equator. Near the poles, just like on Earth, day/night cycles are considerably longer, hence the temperature swings are smaller. Temperature affects 3D printing and material curing to a large extent, and therefore printing machines, processes, materials and habitat location have to be established together, as they affect each other closely. Near-vacuum conditions due to thin atmosphere make the problem even worse, especially if the binder material which is used to solidify Martian regolith is a liquid. On Earth, evaporation behavior of liquids is governed by the presence of water vapor in the atmosphere. However, atmosphere is nearly absent on Mars, and hence no water vapor is present. This would result in deposited liquid rapidly evaporating into the ambient and, immediately afterwards, freezing due to low temperatures.

3. Materials and Methods

3.1. Regolith characterization

The density of regolith was measured inside a measurement cylinder filled with water. Initial water volume was recorded inside the measuring cylinder, which was placed upon the scales. A portion of regolith was then added to water, and weight difference together with volume difference was recorded. From these measurements, density was calculated by $\rho = \frac{m_F - m_I}{V_F - V_I}$, where m_F and m_I respectively stand for the final and initial masses of the mixture, and V_F and V_I stand for the final and initial volumes of the mixture. The average density of wet regolith was 1873 ± 128.4 kg/m^3. This is comparable to the density of wet sand which equals to 1922 kg/m^3. The average density of wet regolith is going to be used as the reference density for comparing the specimen densities and calculating relative densities, which in turn will contribute to analysis of mechanical properties.

Particle size and shape can affect the reaction parameters such as dissolution within the binder, as well as restrictions in temperature and pressure. Small and smooth particles are expected to spread within the binder mass at a higher rate with lower effort, and hence decrease the minimum amount of binder required for paste forming. At the same time, in the conditions where the pressure is low and ambience contains no water vapor, the binder solution evaporation happens at a considerably higher rate. Low temperatures cause preliminary freezing of the binder and halt curing reaction. Large and rough particles might help trap the binder within the paste and prevent it from escaping into ambience and subsequently freezing, thus expanding the temperature and pressure reaction window. Considering that conditions on Mars involve low temperatures and pressures, these considerations are important to take into account.

Regolith particle dimensions were analyzed using dry sieve test. A bulk of regolith was sieved through 125 μm and 63 μm sieves, and the resulting weight percentages were measured. Overall, it can be seen in Table 1 that the majority of particles are smaller than 125 µm.

Table 1: The mass percentage of particles of different sizes from dry sieving tests on a bulk of regolith powder

Sieve size [μm]	**>125**	**63-125**	**<63**	**Total**
Mass [g]	17.38	38.86	26.52	82.76
Mass [%]	21	47	32	100

For investigating the particle shapes, scanning electron microscopy (SEM) imaging was used. Together with SEM, Energy-Dispersive X-ray spectroscopy (EDX) analysis was also performed. Sieved powder specimens were placed upon a layer of carbon paint in order to make the imaging possible and also to fix the positioning of powder particles over the base cylinder, so that contamination of the chamber could be avoided.

From the SEM images (Figure 1), it can be seen that in general particles have irregular shapes, ranging from nearly spherical to highly elongated. Larger the particles are, higher the chance that the shape deviates from sphere. Particles of medium and small size are closely packed, while large particles are mostly located apart from each other (Figure 1). Among the medium and small particles, porosity can be observed, meaning

that liquid can potentially get in between the particles easily without considerable mixing required, and initiate the curing reaction.

(a)

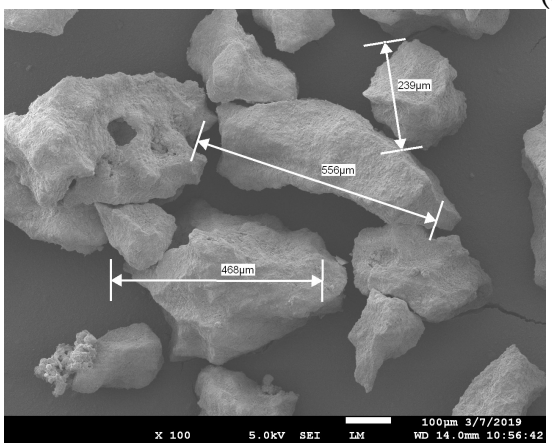

(b)

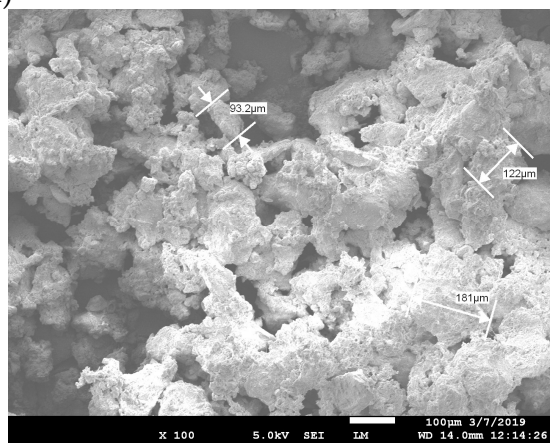

(c)

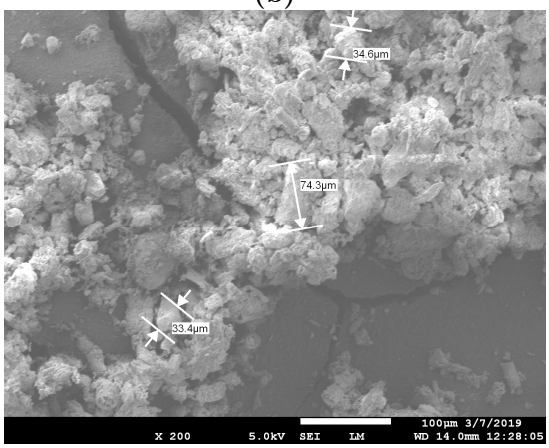

(c)

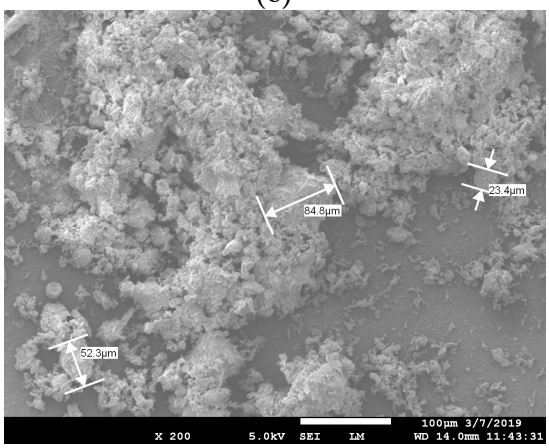

(d)

Figure 1: (a) Mars-simulant regolith powder. SEM images of regolith powder with various particle sizes: (a) large (> 0.125mm) sieved particles (×100), (b) medium (0.063mm < x < 0.125mm) sieved particles (×100), (c) small (< 0.063mm) sieved particles (×200), and (d) unsieved particles (×200).

EDX measurements were also performed during SEM measurements, and the results are presented in Figure 2. The analysis showed a high percentage of carbon and some percentage of gold, which was the result of carbon paint and gold coating, which are necessary for SEM measurements. Therefore, EDX result adjustment was performed and is listed in table of Figure 2, which excluded carbon and gold from calculations. Copper and zinc were also excluded from calculations, as presence of those are a result of carbon paint being too thin or cracked in some locations, As it can be seen from the composition, a large amount of silicate oxide and aluminum oxide is present in regolith, which indicate suitability for geopolymer base, meaning that geopolymer binder can be investigated among other options.

As expected, oxygen is indicated as the most present element, which can be attributed from the fact that regolith mostly consists of various oxides. Among the trace elements, potassium and titanium are detected by EDX, and it is possible that copper, zinc, carbon and gold are among the trace elements as well. Overall, the EDX analysis confirms the composition as indicated by manufacturer.

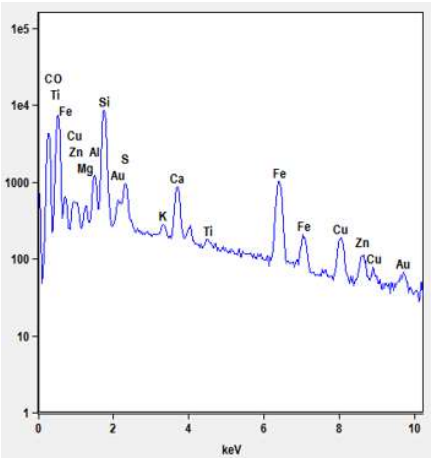

Element	EDX result [%]	Adjusted EDS result (no paint) [%]	Element composition calculated from manufacturers data [%]
O	29.97	62.05	43.07
Si	7.64	15.82	20.53
Fe	6.86	14.20	12.6
Ca	1.54	3.19	5.71
S	0.95	1.97	3
Al	0.87	1.80	6.88
Mg	0.22	0.46	4.2
K	0.13	0.27	-
Ti	0.12	0.25	-
C	46.89	-	-
Au	1.01	-	-

Figure 2: EDX results from a MMS-2 regolith powder sample.

3.2. Binder selection and characterization

Manned Mars exploration has been a research subject for many decades. Among other aspects, potential building materials have been looked at by various articles mostly very recently. Upon the review of these articles, several main options were chosen for the binder trade-off process, as those were looked at the most and seemed most promising. These options were: molten Sulphur [20], Portland cement [21], geopolymer cement [22], and polymers such as polyimides and epoxies [23]. After taking into account several factors such as processing, feasibility for incorporating into 3D printing, state of research, robustness, transportation cost, and total cost, geopolymer cement (Sodium Silicate, $Na_2Si\ O_3$) was selected as the binder material.

3.2.1 Theory

In granular form, Sodium Silicate ($Na_2Si\ O_3$) is a white solid powder with particle size of approximately 0.5-1 mm. The powder has melting point of 1088 °C and density of 2.61 g/cm^3 at 20 °C. This powder is soluble in water, but the solubility highly depends upon the ratio of powder to water and water temperature. The solubility in this context is meant to be complete when the solution is fully transparent, and no undissolved powder particles are visible. Between 25 °C and 80 °C, solubility varies between 22.2 g per 100 ml (18% concentration) and 160.6 g per 100 ml (61.6% concentration). Time is also an important variable when making the binder solutions, because the duration required for dissolution increases as temperature decreases and desired concentration increases. Stirring at 360 rpm and 80 °C temperature was applied to increase solution speed in the binder material.

Geopolymer reaction consists of five major steps, which are schematically demonstrated in Figure 3. For this reaction to initiate, an aqueous alkaline medium (hydroxide or silicate) has to be combined with solid component that includes aluminates and silicates, preferably in powder form. Upon mixing these two components, in this case regolith powder and liquid binder solution, the reaction initiates.

Dissolution is a stage where aluminosilicate particles from regolith powder start dissolving in alkaline medium, provided by sodium silicate solution. As the result of this phase, monomers of aluminates and silicates are formed. This reaction step consumes water to produce the reactive particles. General formulae of this hydrolysis

reactions for aluminates and silicates, where only mass and charge balances are taken into account, follow as:

$$Al_2O_3 + 3H_2O + 2OH^- \rightarrow 2Al(OH)_4^- \quad (1)$$

$$SiO_2 + 2OH^- \rightarrow [Si\,O_2(OH)_2]^{2-} \quad (2)$$

$$SiO_2 + H_2O + OH^- \rightarrow [SiO(OH)_3]^- \quad (3)$$

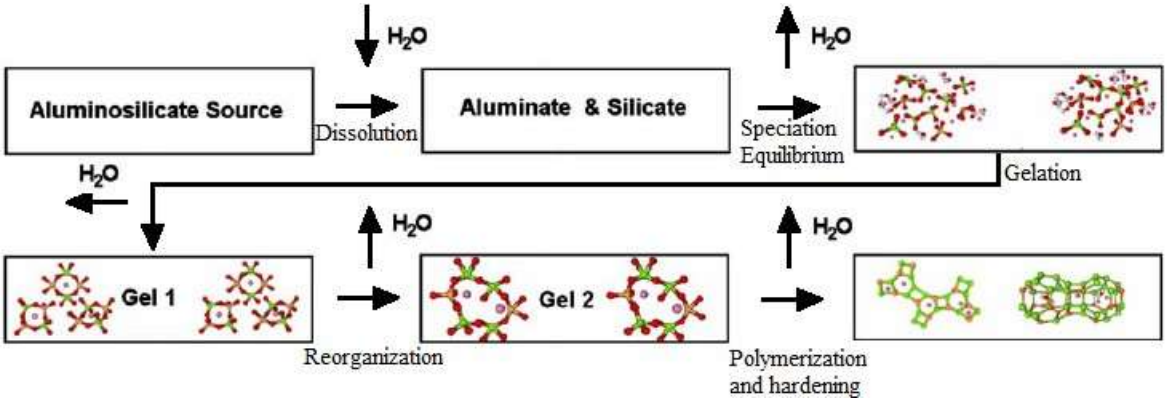

Figure 3: Schematic representation of geopolymerization reaction [24].

Speciation equilibrium, also described as solution saturation in this case, is reached faster with higher pH values. As solution becomes saturated with the particles from the previous step and subsequently oversaturated, aluminosilicate particles combine with each other to nucleate and form small oligomers. During this process, water condenses. It can either evaporate if the reaction occurs close to the surface, or it remains trapped within the pores of material bulk.

Gelation happens as more and more monomers combine together into oligomers, and so mixture becomes less and less liquid. This forms a what is referred to as Gel 1 phase, which consists of a large number of small oligomers. These oligomers continue to react with each other, releasing water into the system, but eventually because of restricted mobility, no nearby connections can be established. At this point, formed oligomers begin to reorganize in order to form more connections within the polymeric network. At the same time, as aluminum particles dissolve considerably faster than silicon ones, the silicon groups continue to dissolve and participate in the polymerization process. This process continues to harden the material bulk, forming a more stable in shape Gel 2 phase. The last stage of the polymerization reaction (with Potassium instead of Sodium, which also can be used for this purpose) is shown in Figure 4. The speed of this phase depends upon ambient conditions and initial component compositions. For

example, unfavorable balance between aluminum particles, silicon particles, alkaline medium and water might lead to gel not even forming in the first place.

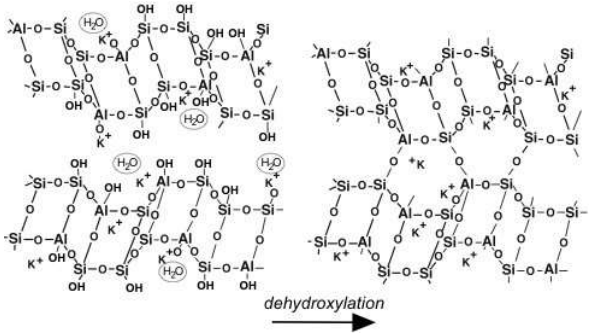

Figure 4: The last step of forming a 3D polymeric network within geopolymer reaction (with Potassium instead of Sodium) [25]

It should be noted that various above-mentioned reaction steps occur concurrently in different locations of the bulk, and do not progress strictly in order simultaneously in the whole bulk [26]. For example, initial gel precipitation starts when the solution in a particular location reached saturation. However, other locations can be still reorganizing to achieve that. This can be viewed from a microscopic image in Figure 5, where in some locations the material still flows to reach destination (mostly on the right), while other locations have reached saturation and have already started gelation phase (mostly on the left). Hence, it is important to provide sufficient time for the mixture to complete the reaction process before using the product, as the overall reaction progression can vary in different bulk locations. Also, varying reaction progression between the regions can introduce inhomogeneity in the bulk, as less links between the regions can be formed in the end.

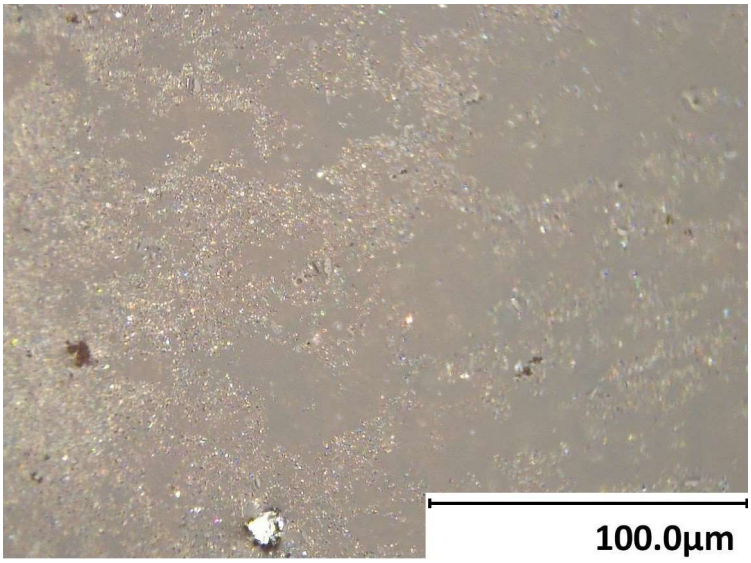

Figure 5: Microscopic image of a mixture surface during saturation and gelation phases (x1000)

3.2.2. Measurements

To investigate the curing reaction properties, differential scanning calorimetry (DSC) analysis was conducted by curing the specimens with the same composition and various temperatures. These temperatures are those at which actual specimens are going to be cured. This DSC analysis allowed for a better estimation of times that initial gelation and final hardening take place, which contributed to the optimal specimen processing. Removing the specimen after the shape is established, but before complete drying and hardening allows for easy removal of the specimen from the mold without the risk of damaging it.

DSC experiments were conducted for the same temperatures that were selected for curing (2°C, 23°C and 60°C). It was expected that low-temperature cure would take a long time, hence the measurement was conducted over night [27]. DSC method used for this measurement consists of decreasing the temperature from room conditions to 2 °C at the rate 5°C/min (default rate), holding the specimen at 2 °C for 12 hr, and heating it up back to room temperature at the rate of 5 °C/min. The second DSC test (at 23 °C) was conducted simply by holding the specimen at room temperature of 23 °C for 4 hr. Knowing that high-temperature cure occurs considerably faster, the selected method was heating up the specimen from room temperature 23°C to 60°C at a

standard rate of 5°C/min, holding it for 2 hr, and dropping the temperature back to room conditions.

3.3. Molding process

Although the research is supposedly concerned with 3D-printing the regolith paste, molded specimens serve as a reference point in result evaluation. Through molding, it is more convenient to see the dependency of mechanical properties of cured specimens on ambient conditions due to lower number of processing parameters. Also, it is easier to change the paste compositions when it comes to molding, as varying thickness of the paste has a very high impact on printing process.

Brick-shaped molds with specimen thicknesses of $t = 5$ mm, width of $w = 10$ mm, and length of $l = 30$ mm were 3D-printed using PLA (polylactic acid) material. Specimens cured at low temperature were stored in refrigerator, specimens for cure at room temperature and pressure were stored in the laboratory, while specimens for cure at low pressure and high temperature were stored in oven with corresponding temperature set beforehand. Low pressure was reached after placing the specimens in the oven. During the second curing stage, while the specimens were still soft but had a set shape, they were removed from the molds.

For the purpose of finding the optimal binder/regolith combination for best mechanical and physical performance, multiple parameters had to be considered to generate a better overview of the properties. In the end, four parameters were selected: temperature, pressure, binder concentration, and regolith-to-binder ratio.

First of all, molding and curing specimens at room condition is the simplest case to perform, as no additional equipment is required. Therefore, basic specimens were also printed in room conditions. Because of this, room condition cured specimens served as a baseline for mixture property evaluation, and higher number of specimens were manufactured for room condition tests as compared to other cases. Regarding the binder and mixture concentrations, there are restrictions that define the boundary conditions. When it comes to regolith concentration, at 70%, the mixture was hardly mixable, and it took significant effort to cover all the powder particles with liquid. At 60% regolith concentration, however, the mixture formed very easily within a couple of stirs, and all the powder was covered in liquid. During the preliminary testing even

lower concentration of 55% regolith was tried, but a lot of cracks were observed after the curing process, and the resulting overall mechanical robustness was very low. Besides, in real applications, it is desired to have as high regolith concentration as possible for reduced transportation costs. Hence 60% concentration was deemed the lowest to be investigated.

Table 2: Specimen composition matrix for curing in room conditions.

Na_2SiO_3 concentration [%] / Regolith concentration [%]	30	35	40	45	50	55
60	2 specimens per each condition manufactured (36 specimens in total)					
65						
70						

The binder concentration boundaries were determined through binder solubility information and preliminary testing. The solution with concentration of 60% was not completely formed after 30 min of stirring at 80°C, and increasing the temperature led to quick liquid evaporation, skewing the resulting concentration. Solution of 55% concentration was able to be formed, but it did not last in completely transparent form for longer than 3 min. This was the highest solution concentration boundary. At 30% concentration, the preliminary testing specimens were mechanically extremely weak after curing, hence it was selected as the lower bound for the tests. After the mechanical testing of specimens cured at 60°C, the binder concentration of 30% was eliminated because of insufficient strength compared to higher concentrations. 55% concentration binder was also eliminated because of fast solution crystallization as well as reduced mechanical properties as compared to 50% solution. As fast crystallization produces unreliable results, it was decided to skip this binder concentration in further experiments.

Table 3: Specimen composition matrix for conditions other than room conditions.

$Na_2Si\ O_3$ concentration [%] / Regolith concentration [%]	35	40	45	50
60				

65 70	1 specimen for each combination (12 specimens in total)

3.4 3D printing process

Molded specimens provided a large variety of data regarding mixture composition properties and their influence at ambient conditions. While some conclusions about the mixture viability can be made from the molding process, it is useful to see how such mixture can perform at similar conditions, but in 3D printing process. The printer used for this project was Automated Dispensing Robot TSR2301 (Techcon System, US), (Figure 6a). Primarily used for dispensing fluids, as it can operate within 3 axes, it was used as a binder deposition 3D-printer after making some adjustments.

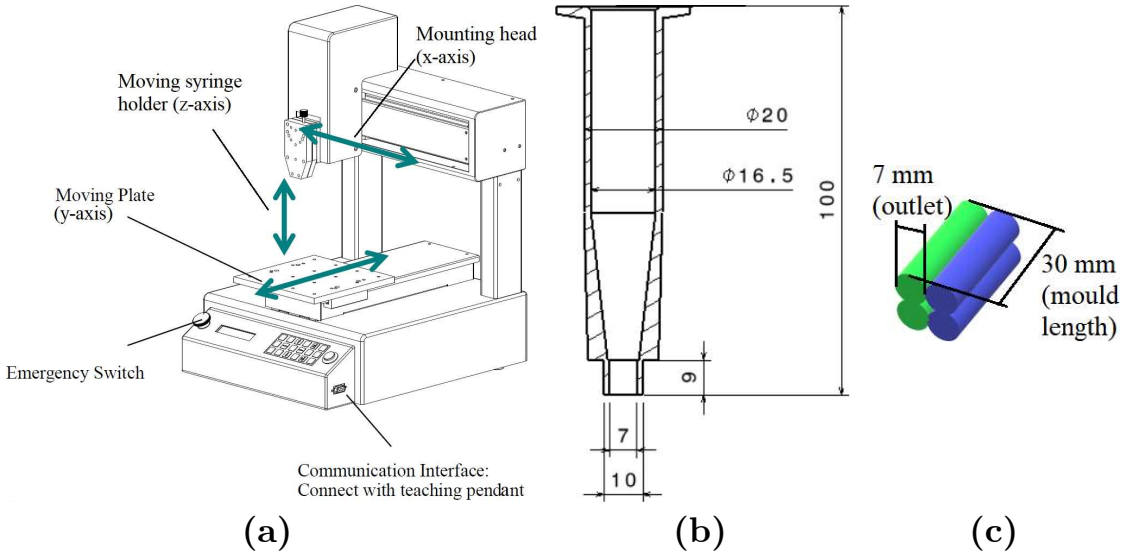

Figure 6: (a) Schematic representation of selected printer model with key components indicated [28], (b) Redesigned extruder syringe, and (c) Printing pattern for the 3D-printed specimens. Green lines are printed towards the front, while blue lines are printed towards the back. Top two levels are either deposited immediately or after 30 min delay, to test the mechanical property dependence on deposition delays.

First of all, the viscosity of the paste is of vital importance when it comes to printing, especially with such limited outlet diameter. Low viscosity mixture (65% regolith and below) did not hold the shape upon deposition at all, flowing all over the build plate. Mixture with the lowest possible regolith ratio that could hold the programmed shape was the one with 66% regolith concentration, which set the lower boundary for printing.

Because of rapid viscosity change with respect to regolith ratio, going up to 69% regolith content resulted in a paste that was too thick to be printed even with the largest syringe diameter possible (7 mm), Figure 6b.

The syringe provided by manufacturer (with maximum 3 mm diameter) was redesigned in order to achieve two goals: increase syringe outlet diameter, and increase the slope inside the syringe, as horizontal bottom wall of the originally provided syringe causes the material to be pressed against it and cure under pressure instead of being pushed into the outlet. The issue of rapid mixture curing under pressure complicated the printing process significantly. Although syringe redesign helped to partially alleviate the issue, the problem was not completely fixed. The issue was alleviated by significantly increasing the outlet diameter and decreasing mixture viscosity, but the latter option is limited because its leads to inability of the deposited paste to keep its shape upon deposition. The best combination of deposition conditions that could be achieved was deposition at 0.3 bar pressure provided by the fluid dispenser, with the outlet diameter of 7 mm.

The specimen printing pattern consisted of four lines, two next to each other with two more placed on top (Figure 6c). Two separate sets of printing programs were created. The first was printing all the four lines in one go, while in the second program, a delay was allowed between the first and second layer of deposition. This variation can provide information about the impact of printing duration on mechanical properties of resulting part. Theoretically, having layers deposited with a delay causes them to have different progressions in their curing process, which can introduce inhomogeneity into the material bulk through not allowing polymeric links between the layers to form. Potential decrease in mechanical properties of the specimens printed with delay can potentially lead to the conclusion that printing has to be done as fast as possible or with specific designed printing paths to ensure good properties. When it comes to the printing projects of large scope, namely habitats, the inevitable printing delays might create issues and hence have to be taken into account.

3.5 Mechanical tests

Elastic modulus is defined as a ratio between applied stress and specimen strain. In the case of three-point bending test, elastic modulus can be determined by taking a linear

portion of force-displacement curve in the there-point bending test (Figure 7), and then dividing the force values into stress using three-point bending formula for stress:

$$\sigma = \frac{3Fl_s}{2wt^2} \tag{4}$$

where F is the applied force value, l_s is the testing bench span, w is the specimen width, and t is the specimen thickness. The displacement d was converted to strain values using equation $\varepsilon = \frac{d}{t}$.

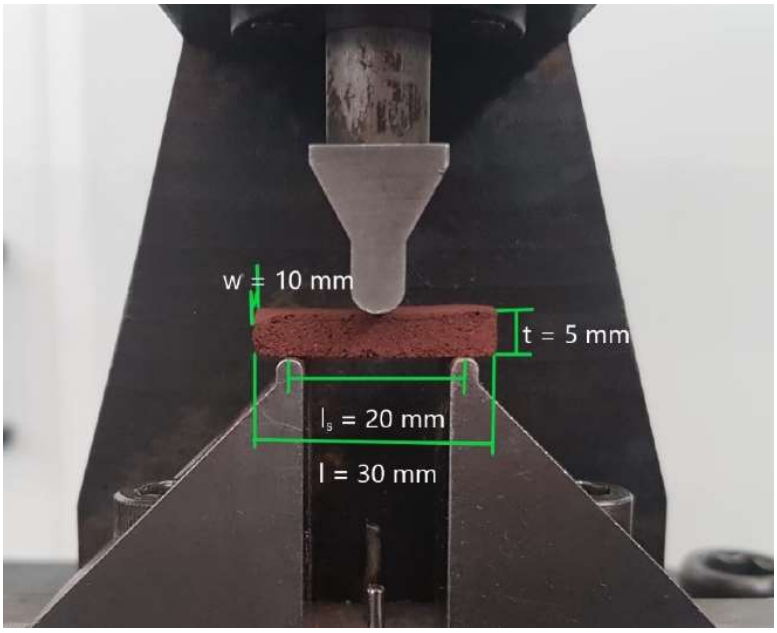

Figure 7: Three-point bending test setup

4. Results

4.1 DSC results

From the obtained plots for 2°C (Figure 8a-b), the reaction seemed to be completed within 100 min from the start of experiment, which can be explained by a very small specimen size (~11 mg). After 100 min, the curve becomes almost horizontal. Figure 8b covers the part of the result plot which contains the reaction space. As it can be seen, the second part of curing (hardening) lasted for 92 min. The first part of cure happened considerably faster as it can be seen in Figure 8a which covers the very beginning of experiment. The increase in heat flow happened within 2 min, which is quite fast.

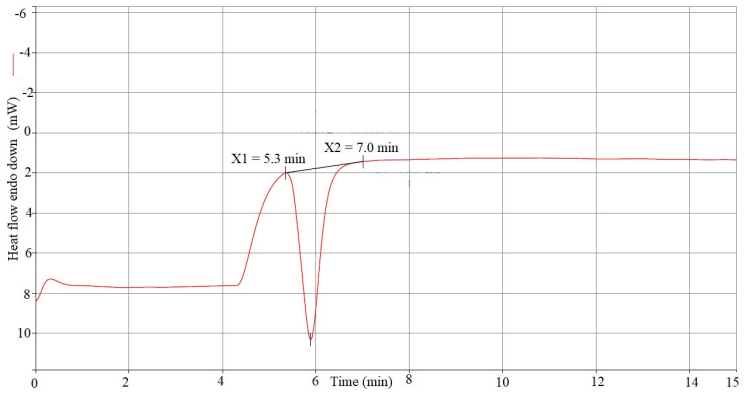
X1 = 5.3 min
X2 = 7.0 min
Heat flow endo down (mW)
Time (min)

(a) 2°C

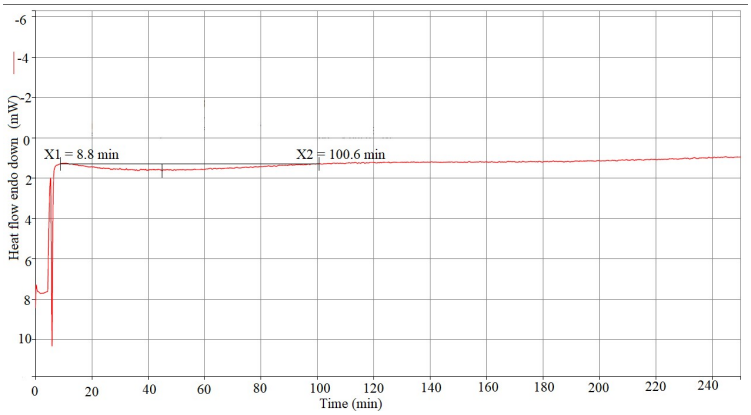
X1 = 8.8 min
X2 = 100.6 min
Heat flow endo down (mW)
Time (min)

(b) 2°C

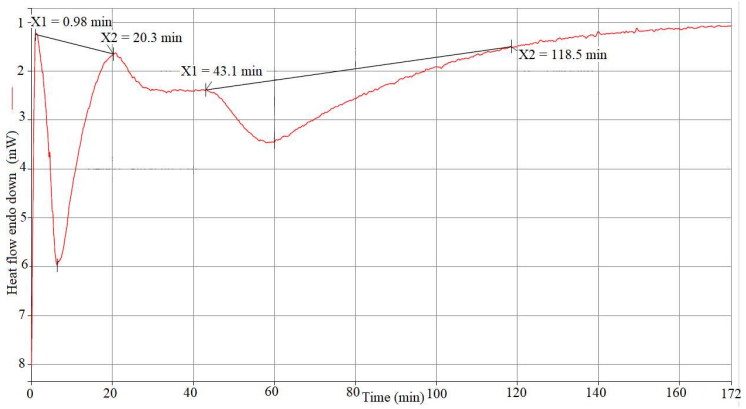
X1 = 0.98 min
X2 = 20.3 min
X1 = 43.1 min
X2 = 118.5 min
Heat flow endo down (mW)
Time (min)

(c) 23°C

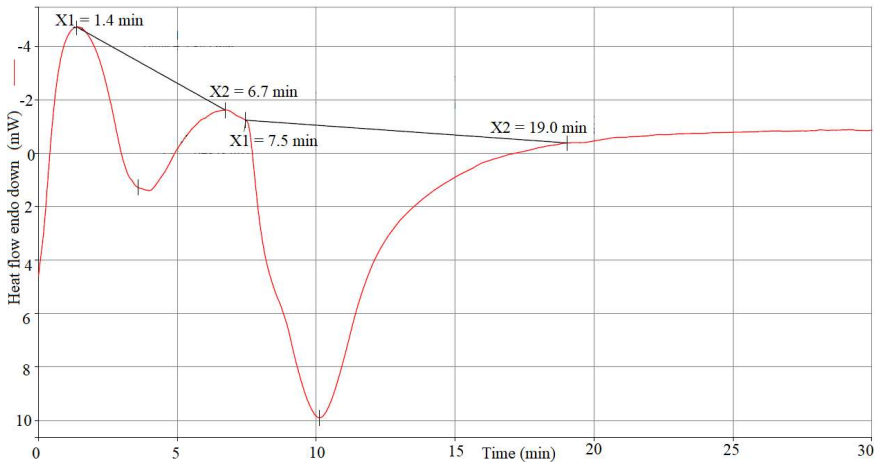

(d) 60°C

Figure 8: Complete DSC plot for curing the specimen at (a-b) 2°C, (c) 23°C, and (d) 60°C, including analysis of both cure steps.

The result of 23°C case, from the start until the point of curve straightening, is shown in Figure 8c. Unlike in the case with low temperature, the first gelation phase starts almost immediately upon loading the sample in the DSC apparatus, as the beginning of the drop is at 1 min. Seemingly the first phase here lasts longer (19 min) than in the case with low-temperature cure. After that, the second phase lasts for approximately 1 hr. It is important to note that the specimen size in this case was approximately 21 mg, which could explain the duration of the first phase. As it can be seen in Figure 8d, the reaction of 60°C was completed under 20 min. The first gelation step ended within 5 min, while the second gelation phase lasted for 13 min only.

The results show that the second gelation phase, or hardening of the mixture, occurs considerably faster at higher temperatures. Indeed, in this phase, oligomers rearrange themselves in order to find more available connections and form a complete 3D network, where mobility plays crucial role. For the first phase, however, this dependency does not seem to be the case. Looking at the beginning of DSC results for low-temperature cure (Figure 8a-b), it can be noticed that the curve starts with a straight line, while the other two plots start with a sharp rise. It can be explained as follows: as the curing for 2°C specimen started at room temperature and then the temperature dropped, the heat flow change from the temperature drop cancelled out the curve part related to the first stage of the curing. Regardless, looking at the reaction, it is clear that the first gelation stage, where small oligomers form, depends

more on the concentrations of necessary components and alkalinity of the mixture, and temperature is not as important due to assumed homogeneous distribution of the components. The reaction there can occur straight away, without much movement necessary.

4.2. Molded specimens

4.2.1. Physical properties

A stark contrast between different specimens already arose during their removal from molds. In fact, one of the reasons to remove specimens during the curing process and not afterwards was the danger of destroying the specimens. This was especially noticeable when curing the specimens in the oven at high temperature (60°C). In addition to hardening, the specimen also expands at temperatures higher than it was during deposition, which was done at room temperature (23°C). This made the specimen not removable from the mold without forcefully separating it from the walls with a thin object like razor. The specimens were removed from the mold during the second stage of curing, the timing of which was derived during DSC analysis. During the first reaction stage, the mixture is not yet gelated, meaning it loses shape upon the attempt to remove it.

When it comes to curing time, temperature is the detrimental factor, while pressure seems to have little to no effect on it. While curing specimens at 60°C, it was easy to see that total curing time took around 6 hr for all three different pressure conditions. The state of specimen curing after 6 hr was identical by the end of this time, and the progress was checked every 30 min. In comparison, total curing time for room temperature specimens took around 30 hr. Total curing time for specimens at the lowest temperature (2 °C), took 72 hr, which is considerably longer.

Porosity of the specimens was directly related to curing pressure of the specimens, as it can be seen in Figure 9. Curing completed at atmospheric pressure (Figure 9a-c) did not induce any visible porosity in the specimens. Specimens cured at 0.1 bar (Figure 9d-e) have small uniform pores through all the specimen material. Specimens cured at even lower pressure 0.01 bar (Figure 9f-g) have several large pores instead of a large number of small ones. Additionally, surfaces of these specimens are rugged and irregular. Significant increase in visible porosity of the specimens cured at decreased pressure can be explained by the rapid decrease of the boiling temperature of the

mixture as the pressure is decreased. Decreased content of moisture in ambience resulting from vacuuming process causes the liquid present in the mixture rapidly evaporate. This can explain the difference between pores in the specimens: slightly lowered pressure (0.1 bar) makes boiling slower and less rapid, generating small and uniform bubbles. Very low pressure (0.01 bar, slightly higher than Martian pressure) on the other hand causes the boiling process to be very rapid, making bubbles large and also making the surface of the specimens rugged.

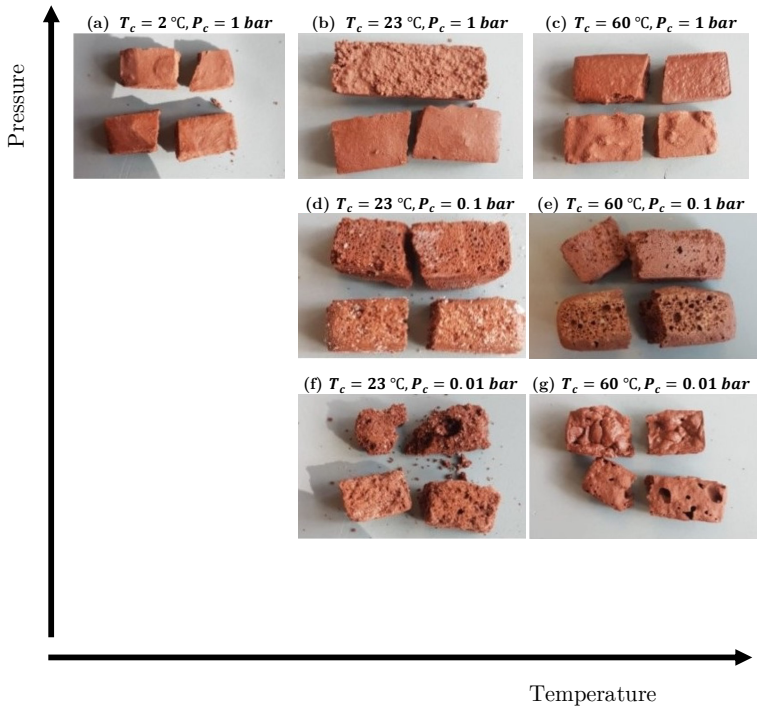

Figure 9: Specimens manufactured under different environmental conditions

Change in the relative density of molded specimens with respect to change in Na_2SiO_3 concentration, regolith percentile, pressure, and temperature can be seen in Figure 10. Increasing the Na_2SiO_3 concentration in ambient pressure and P=0.1 bar increased the relative density, while it had negative effective at P=0.01 bar (Figure 10). In general, increasing the temperature decreased the relative density of the final product (Figure 10). Higher temperatures force evaporation occur faster and improves overall molecule mobility, so during the cure process, when mobility of the oligomers is still present, more residual water molecules are able to escape the material bulk and evaporate.

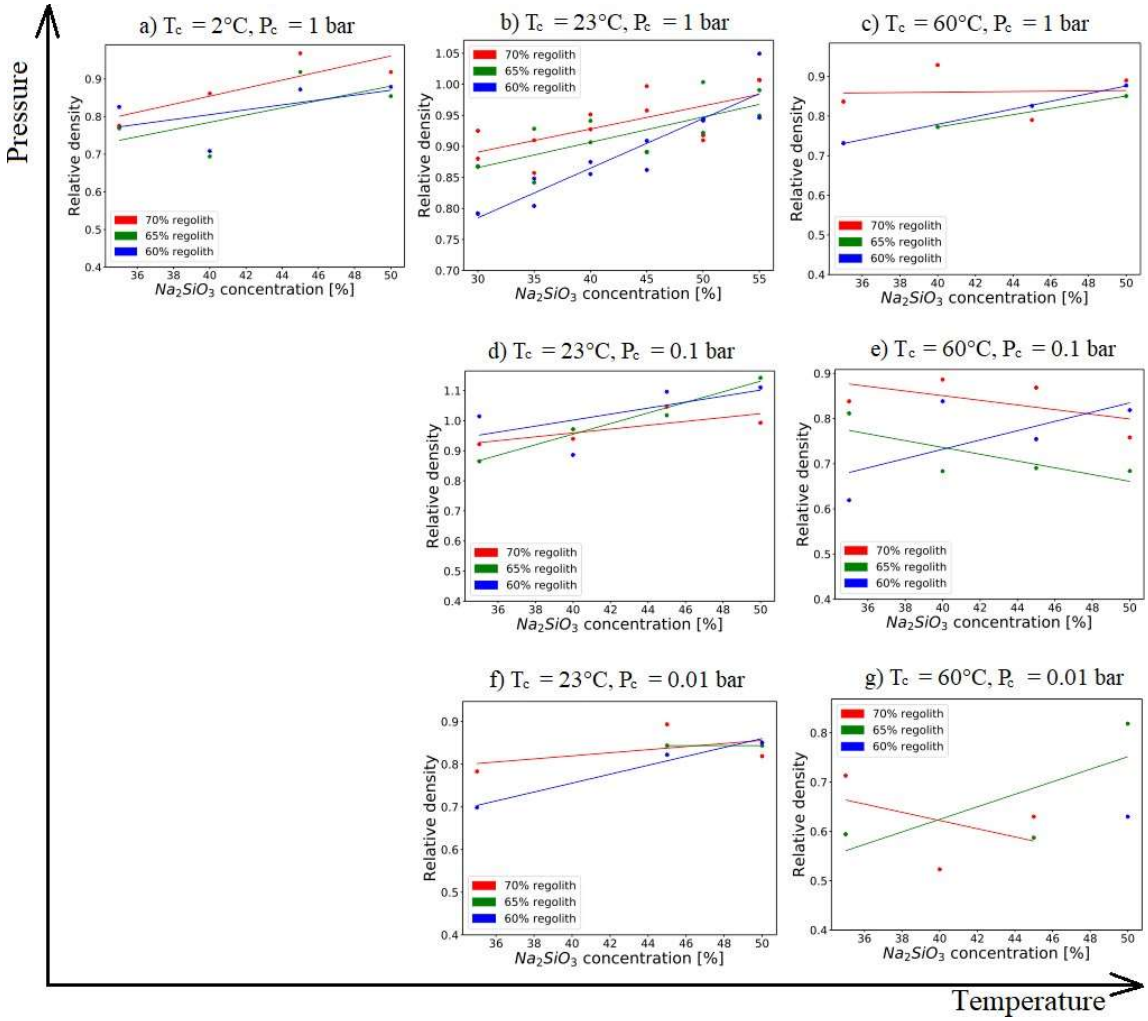

Figure 10: Comparison of relative density values for molded specimens

For better information about pressure effect on density, tests at more conditions would be useful for the results to be more conclusive. At high temperature, clearly, lowering the pressure decreases the density as water present in the mixture was forced to evaporate into near-vacuum ambience (Figure 10). This creates pores, which become permanent in the bulk of material because of fast curing times. These pores are visible with naked eye in Figure 9g. However, as shown in Figure 10, such dependency may not be the case for other temperatures. While 0.01 bar pressure specimens still show the lowest density, specimens cured at 0.1 bar have clearly highest average relative density (Figure 10). Potentially, this could be explained by the balance of reaction rate and vacuum-induced boiling rate. The specimens cured at 0.1 bar pressure in room temperature have very small pores (around 0.1-0.5 mm), while 0.01 bar pressure specimens have large ones (1 mm). Perhaps when the reaction rate is slow enough (in

lower temperatures), there is enough time for the curing oligomers to move and fill the space freed up by boiling process. This reduces water amount in the specimens and also reduces the number of pores. At lower pressure (P=0.01 bar), however, the pores are simply too large to be easily filled by curing material, as mobility of oligomers is not unlimited. To further test this claim however, more tests have to be done the wider range of temperatures and pressures.

On average, it seems that lowering the amount of regolith decreases density of the specimens. This can be easily explained by increased water content, as less regolith means higher binder solution amount in the mixture. Overall higher amount of water means that more specimen mass can be lost to the ambience in the form of water, decreasing the density. Same reasoning can be applied to the Sodium Silicate concentration within the binder solution, where lower concentration means higher water content that is free to be evaporated.

4.2.2. Elastic modulus

The elastic modulus values of specimens molded in different conditions are compared in Figure 11. It should be pointed out that some of the plots have a small number of data points. As indicated in Figure 9, specimens cured at certain conditions were extremely fragile and broke either during mold removal or upon pre-loading part (0.5 N) of the three-point bending test, hence those specimens can be considered as failed specimens.

As it can be seen in Figure 11, increasing the temperature clearly causes the elastic modulus to rise. The difference in elastic modulus for 1 bar pressure between low and room temperature is not large (20 MPa), while the difference between room temperature and high temperature for all pressures is very large, ranging from doubling for 0.1 bar pressure to quadrupling for 1 bar pressure. High temperature increases the mobility of the oligomers, allowing them to interlink into polymers more reliably. This causes the stiffness to rise, as an interlinked polymer is considerably less mobile than a collection of oligomers that can slide along each other.

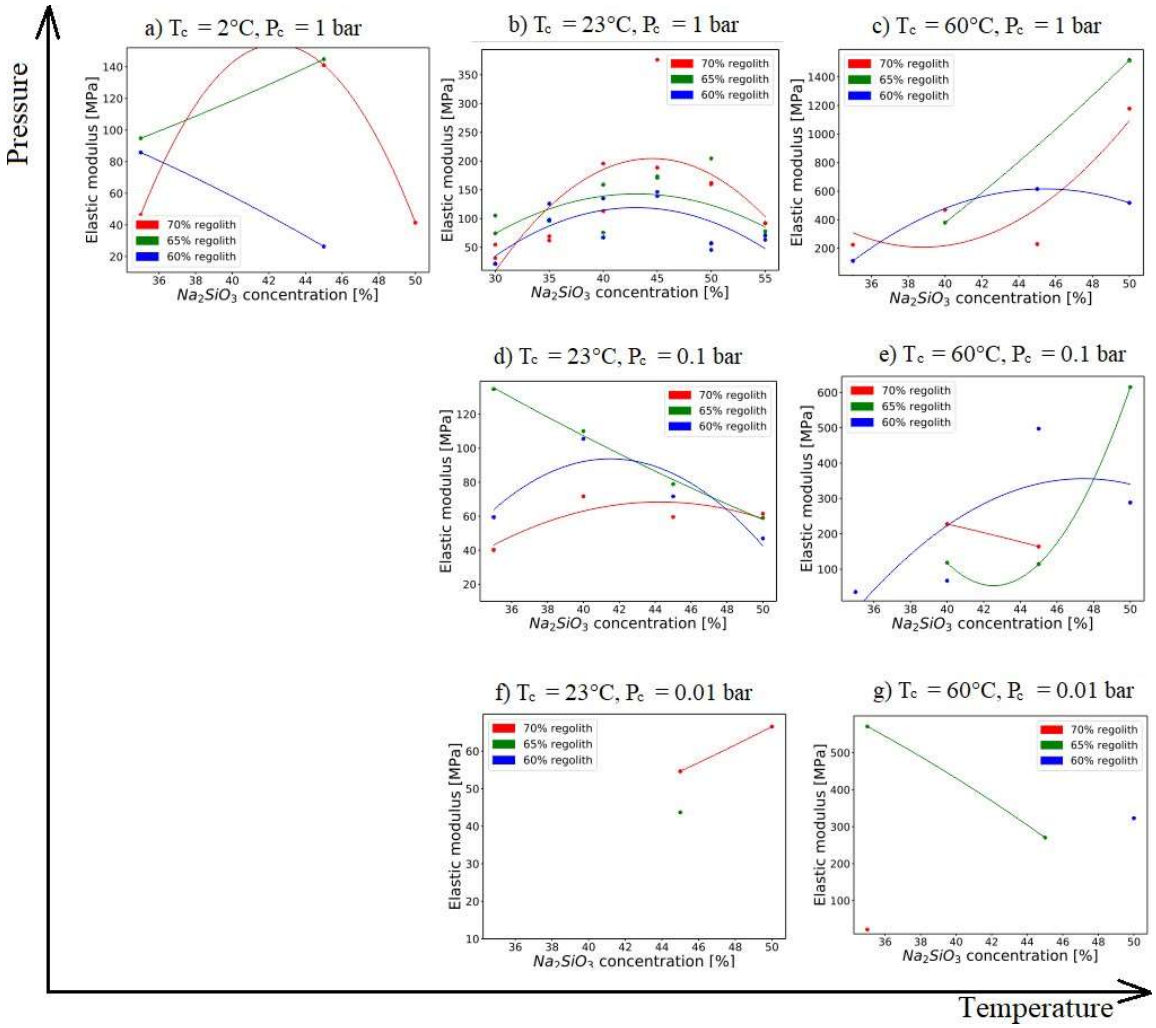

Figure 11: Comparison of ultimate flexural strength values for molded specimens

When it comes to pressure, elastic modulus decreases with the drop of pressure (Figure 11). For instance, at 60°C, the average stiffness of the specimens manufactured at 1 bar is almost twice of those made at 0.1 bar. Similar to the reasoning mentioned for temperature effect, the presence of water during the curing allows for better interlinking into large polymeric chains, increasing elastic modulus. As the pressure is decreased, water evaporates and restricts mobility of oligomers during the curing process, halting polymerization. Between 0.1 bar and 0.01 bar, nearly all the water evaporates quite fast with the only difference being the size of pores. This might explain the similar elastic modulus values for both pressures, as the duration of window for polymerization

is reduced similarly. As smaller amount of polymeric chains allows oligomers to move along each other during stress application, the elastic modulus drops.

4.2.3. Ultimate flexural strength

The ultimate flexural stress (UFS) values for each of the molded specimens are plotted in Figure 12. Clearly, curing temperature increase directly increases the maximum flexural stress endurable by the part. High temperature allows for higher oligomer mobility and reaction rate, which increases the amount of polymeric links and hence makes the material stronger. The increase in UFS values between temperature steps at each pressure ranged from 83% (like between 23°C and 60°C at 1 bar pressure), to 425% (like between 23°C and 60°C at 0.01 bar pressure). This is in accordance with what was observed for elastic modulus (Figure 10). Faster water evaporation is also an effect of high temperature. Water emitted during the curing reaction in high temperature ambience is removed from the pores through faster evaporation, however vacant space can be filled by the material assuming it is in the process of reacting and is mobile enough, which high temperature allows. This decreases the volume of non-functional space in the material bulk (pores become filled), and this increases the overall strength.

Decrease in pressure induces rapid water evaporation. This generates pores, which are larger for lower pressure values, and destroys reaction medium for link formation. The formation of large pores decreases the effective volume of material bulk, as pores and unreacted particles do not contribute much when it comes to mechanical properties. Decrease in elastic modulus supports this observation as well.

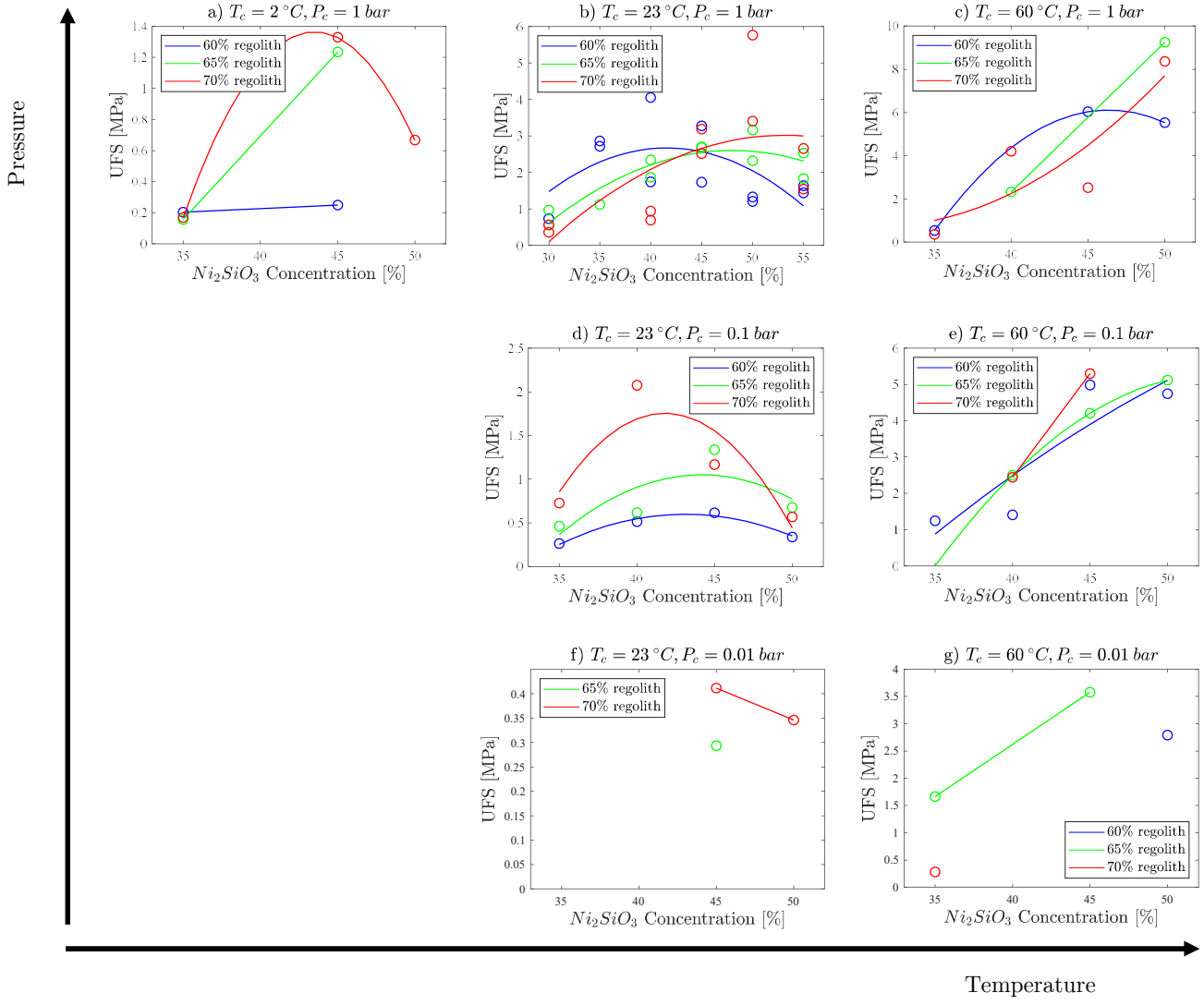

Figure 12: Comparison of ultimate flexural strength values for molded specimens

4.3 3D printed specimens

4.3.1 Physical properties

During the curing process of the printed specimens, the deposited mixture was flowing over the build plate as no walls were present to restrict the movement. This caused irregularity in dimensions as it can be seen in Figure 13. The printing process with small outlet diameter creates an issue related to pressure required for mixture deposition. Applied pressure causes the part of the mixture that does not get deposited to rapidly cure, solidifying it in the process and making it unsuitable for further printing. Roughly same amount of mixture was prepared for each specimen print (10-11 g), but the mixture amount that was actually deposited for each specimen varied.

This effect can be observed by comparing Figure 13d and Figure 13e, where in the specimen shown in Figure 13d, less mixture was deposited in the second layer, while in specimen shown in Figure 13e, the first and second layers are both deposited similarly. By using large syringe outlet diameter, the paste can be deposited under smaller pressure.

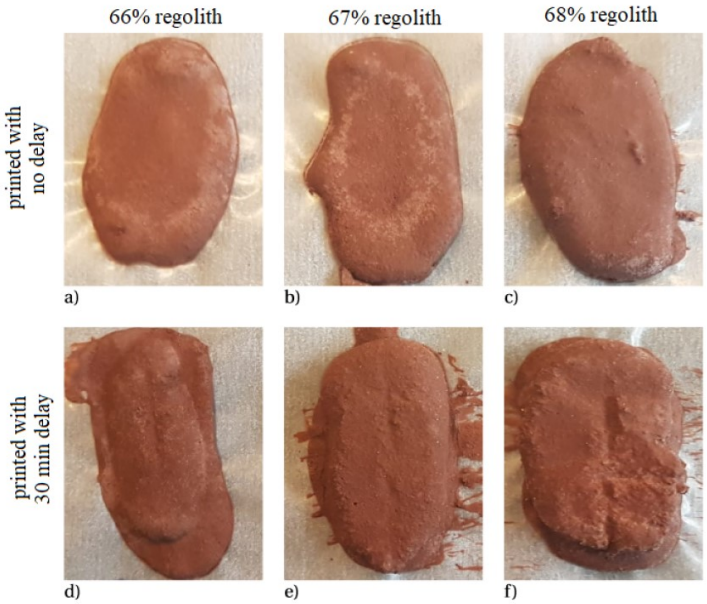

Figure 13: 3D-printed specimens with different compositions and with/without delay

As for the differences between printing the whole specimen in one go and printing it with a delay, the difference is clear even visually. Specimens without delay (Figure 13a-c) were spread over the deposition plate to a larger extent, and they were thinner as compared to their counterparts (Figure 13d-f). Specimens with printing delay had a clear border between the layers. This indicates that the curing reaction that partially completed in the first deposited layer progresses far enough that the second deposited layer does not get fully incorporated, and mechanical properties at the border between the layers are likely different than inside the layers. If this phenomenon affects overall mechanical properties negatively, which is likely because of introduced inhomogeneity, it provides more argument in favor of increasing syringe outlet diameter when designing 3D-printing equipment.

Relative density, elastic modulus, and UFS of the printed samples at room temperature are compared to average values of molded specimens in each temperature and pressure

condition in Figure 14. Printed specimens clearly have higher density values as compared to molded specimens (Figure 14). During the printing, the mixture was free to flow on the build plate where it was deposited. Inside the mold, there was less space available for mixture mobility. Hence, after the printing, the mixture had more freedom to rearrange into a more compact and efficient packing, increasing packing density considerably. This mobility was combined with higher surface area for water evaporation. Because of relatively low curing temperature (room conditions), density increased as water was evaporating and allowing oligomers to fill the space. With delayed second layer printing, there was even more opportunity for water to evaporate as essentially some extra water had evaporated from the first layer before the second deposition, making density even higher.

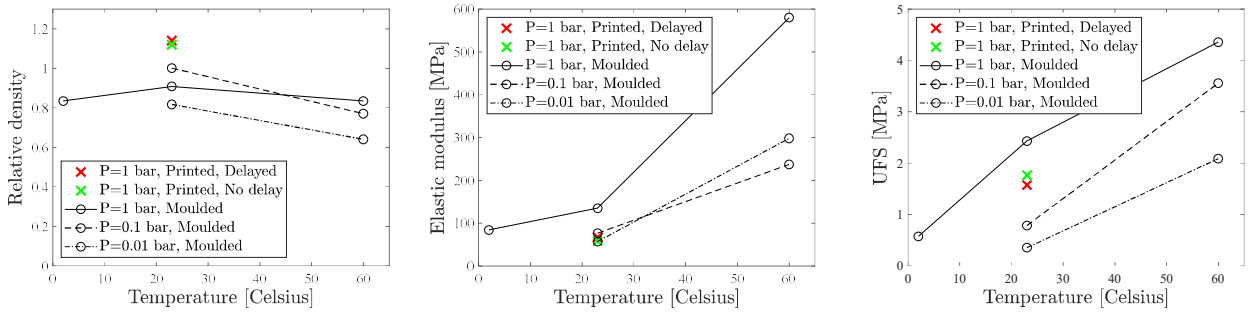

(a) (b) (c)

Figure 14: Average (a) relative density, (b elastic modulus, and (c) ultimate flexural strength (UFS) for all the specimens at different temperature and pressure conditions

4.3.2. Elastic modulus

Looking at the average values of the results of the molded specimens and the 3D printed specimens in Figure 14b, the elastic modulus of specimens printed at room conditions are much lower than their molded counter values, and they are close to the elastic modulus of specimens molded at low pressure (58 MPa for delayed specimens and 65 MPa for non-delayed on average as compared to 134 MPa for molded specimens). During molding, mobility of the mixture is very limited, and deposition is performed very fast by pouring the material. Printing introduces a delay while the syringe is working (programmed printing duration was 8 seconds), and the mixture spreads over deposition location afterwards. This induces the variations in reaction progression across different bulk locations. While parts of the mixture are flowing and rearranging

to achieve optimal packing, some other parts are already settled, and reaction is progressed further. Between the particles from locations with different reaction progress, less oligomers can interlink, hence reducing the amount of polymeric links and decreasing elastic modulus. The stiffness of specimens with delayed layer deposition is higher than those printed in one go, as more water manages to evaporate from the specimen bulk. This restricts the mobility of oligomers during stress application.

4.3.3. Flexural strength

The flexural strength trend (Figure 14c) is similar to elastic modulus trend (Figure 14b). At room conditions, average highest achieved flexural stress of printed specimens is 70% of the value for molded specimens. The lack of boundaries around the deposited mixture allow the paste to flow in different directions, changing the reaction progression extent across the material bulk. This reduces the amount of polymeric links formed, as the curing material is not as homogeneous as molded specimen. Delay between printing the layers makes the bulk even less homogeneous, decreasing flexural strength.

5. Discussions

5.1. Viability of the products

Looking at the result as a whole, the proposed binder/regolith geopolymer mixture looks decent, especially considering the flexibility of binder composition, even though it was out of the scope of this research. A large issue arises when considering the fact that for 3D printing being applicable on other celestial bodies, ability to cure well in low pressure and temperature conditions is crucial. From this point of view, the mixture is not suitable for space application, at its current form. An overview of explored curing conditions and their effect on the resulting material properties is shown in Table 4.

The role of water in the curing process of geopolymer mixture is crucial. It is necessary for the hydrolysis of powder particles, and then it gets emitted during polymerization process and provides the medium for polymerization to occur. Decreased pressure causes water to rapidly evaporate and leave pores in material bulk, which ends curing reaction prematurely and introduces inconsistency in the material bulk. Increase in temperature can help bypass the rapid loss of water by speeding up the reaction. However, a combination of low temperature and pressure yields materials that are hardly useful for construction purposes. In this project, performing experiments with specimens cured at low temperature (2°C together with reduced pressure 0.1 and 0.01

bar) was not possible. Nevertheless, the results for very low pressure even at high temperature is not sufficient.

Table 4: Viability of tested specimens with respect to cure conditions. Green cells indicate good conditions, yellow indicate conditions that produce somewhat useful material, red indicate poor cure conditions.

T_c [°C] / P_c [bar]	2	23	60
1	◦ very low mechanical properties ◦ low robustness ◦ no porosity ◦ long cure time	◦ good mechanical properties ◦ good robustness (most compositions) ◦ no porosity ◦ medium cure time	◦ good mechanical properties ◦ decent robustness (most compositions) ◦ no porosity ◦ fast cure time
0.1	N/A	◦ poor mechanical properties ◦ good robustness ◦ some porosity ◦ medium cure time	◦ decent mechanical properties ◦ decent robustness (most compositions) ◦ high porosity ◦ fast cure time
0.01	N/A	◦ poor mechanical properties ◦ unacceptable robustness ◦ high porosity ◦ medium cure time	◦ decent mechanical properties ◦ low robustness ◦ high porosity ◦ fast cure time

Another component property that strongly affects the mechanical properties is the ratio between silicon and aluminum in the mixture. Mechanical strength, porosity, and elastic modulus all depend on this ratio. If the Si/Al ratio is low (below 1.4), the microstructure of the resulting cement is reported to be highly porous and inhomogeneous, resulting in inferior mechanical properties. The ratio above 1.9 shifts the particle balance in another direction, lowering the mechanical properties as the ratio goes further up. By staying in the ratio range of 1.65 and 1.9, the porosity is low and material bulk is largely homogeneous, which translates into high mechanical strength and elastic modulus. Such behavior can be explained by chemical balance between the particles, where skewed particle ratios result in high number of unreacted particles, creating defects inside the final product.

In this paper, optimal silicon to aluminum ratio seemed to be achieved at 45% binder concentration mixed with regolith at 70% regolith to binder ratio. Modifying the binder mixture by for example adding a hydroxide might shift the balance as well, for better or for worse. It is important to track this ratio in order to optimize the mixture properties and ensure the best possible performance.

In the current binder composition iteration, a large amount of binder with respect to regolith is required to incorporate all of the powder into a mixture. Lowest ratio of binder to regolith that was achieved was 30/70, and the resulting mixture was very viscous and inconsistent at times. Such ratio is very high when it comes to transportation costs of the binder from Earth to Mars. While potentially required elements can be extracted from various sources on Mars and processed into binder components, technologically such idea is far from being possible. From this point of view, it is required to modify the binder composition in such a way that a considerably lesser quantity of it is necessary.

When it comes to printing, a lot of phenomena come into picture that complicate the process. It was found out that the mixture becomes compressed and rapidly reacts under pressure during deposition, which makes it unprintable. This was expected for such a reaction, as oligomers are forced to reallocate into the most compact structure possible, reacting with each other. This effect caused the mixture to be deposited unevenly, skewing the results and complicating printing process. Delays between the layers deposited by printer also affect the properties in a negative way, as the material bulk becomes inhomogeneous. Viscosity of the mixture is highly dependent upon the regolith content, and even a difference of 2% makes a significant difference when it comes to printing. Limited outlet diameter of the syringe that could be achieved during the project (7 mm) also limited the ratios of regolith to binder that could be used to obtain data. As expected, changing manufacturing method from molding to 3D-printing introduces multiple issues that have to be solved during mission design.

5.2. Geopolymer binder improvement

When it comes to degree of regolith powder processing, smaller particles allow for faster overall dissolution of aluminosilicate particles in aqueous medium. The powder used in this research was preprocessed into fine size particles before packaging and shipping, meaning the dissolution during the mixture creation is fast and homogeneous. However,

in real application conditions, regolith powder on Mars might contain very large particles together with small ones, increasing not only the dissolution speed, but introducing further reaction speed discrepancy between the various regions in the material bulk. This might lead to non-homogeneous final properties, which is not good for overall mechanical properties. This is easy to bypass however, as a grinder machine can be used in order to reduce the overall particle size, potentially together with sieving machine.

Optimally, the binder should include a strong base as one of the components, for example Sodium hydroxide $NaOH$. It serves multiple purposes in the geopolymer mixture, namely introduces easily accessible hydroxide particles OH^- which can be incorporated in the monomers, increase alkalinity of the mixture speeding up the reaction, and also act as a catalyst during the gelation phase. However, for the purpose of this research it was decided to omit the usage of hydroxide. First of all, working with a strong base is more dangerous, and considering experiments with 3D printing where pressure is involved are required, mishandling the solution could potentially have negative influence on the printer and surroundings. Also, a large number of specimens is planned to be made at the same time, and making solution with one soluble material is faster and more convenient. Adding a base into the picture also would introduce another variable in the specimen matrix, yielding less useful information in the end due to time restrictions. Overall, using a simpler solution provides better baseline results for figuring out the dependency on the main variables of the reaction: temperature and pressure.

Expanding on the previous point, higher alkalinity does not always directly improve the resulting mixture properties [29]. In fact, high alkalinity induces the formation of $[SiO_2(OH)_2]^{2-}$. The former particles tend to form smaller oligomers with $2Al\,(OH\,)_4^-$ and halt further polymerization, while the latter allows for more links to be formed and hence increase the size of the resulting polymer. This means that the balance between $[SiO_2(OH)_2]^{2-}$ and $[SiO(OH)_3]^-$ particles directly impacts mechanical properties of the formed geopolymer cement, which in turn directly correlates to the alkalinity of the solution. This is one of the reasons why typically a combination of a base and a silicate is used over a pure hydroxide.

5.3. Application to Mars

In current iteration, the mechanical properties of the mixture after being cured in either low pressure or low temperature are unsatisfactory, and it is safe to assume that combining low temperature and pressure to simulate Martian conditions would make the situation even worse. Low pressure has to be counterbalanced by significantly increasing the reaction rate, which is done by either high temperature or modification of the mixture. Low temperature has to be counterbalanced by helping the particles to arrange into efficient packing, which is done by either increasing pressure or, again, modification of the mixture.

When looking at potential solutions in the context of Martian application, increase in temperature can be achieved by choosing a landing location where highest temperatures are achieved (around 20°C). This temperature is achieved in equatorial regions during the Martian midday in summer. However, curing process takes well over 24 hr, and day on Mars lasts 24 hr 37 min, meaning the lowest temperatures as expected during the night also will be present over the course of curing. Hence, additional heating mechanism is required. This can be done in the form of lamps radiating heat or creating an enclosed dome which can also provide pressure increase. The former option consumes a large amount of energy, but otherwise requires little equipment to be used. The latter option requires a dome that is larger than a planned building, which required a very large amount of resources to be brought/made. Heating lamp or even a sintering laser can be viable solutions to this problem. The dome, assuming it would be used for printing purposes only, seems like too large of an investment to be justified. Overall, in order to reduce the amount of resources during 3D-printing on Mars, the binder mixture has to be modified with at least adding a hydroxide into the mixture, as suggested in the literature. It must be noted that experimental tests and/or numerical simulations must also be carried out to investigate high-speed impact resistance of the selected printing materials to small space objects. Explicit finite element approaches have shown promising results in high-speed impacts [30-34].

When it comes to printer design, a crucial parameter that has to be maximized is the outlet nozzle diameter. Large diameter allows for thicker paste, which reduces the amount of binder required and decreases the flow, allows for lower deposition pressure, which is needed to keep the paste uncured, and allows for layers of higher thickness to be deposited, which increases mechanical properties of the complete structure. It is worth noting that the delays between layer deposition are inevitable because the

structure to be printed is of a size of a building, making printing process considerably longer than printing small laboratory specimens. The printer for space mission is expected to be designed from scratch, so incorporating as large nozzle diameter as possible should not create issues.

6. Conclusions

In this paper, a geopolymer mixture with the implementation of Martian regolith was investigated as a potential constructing material for a Martian base. The goal of this research was to study the effect of reduced temperature and pressure on the physical and mechanical properties of cured geopolymer material. The other objective was to look at the properties of the geopolymer mixture with respect to 3D-printing, as this is the manufacturing method that looks very promising when it comes to space construction without human interference. The results of testing the specimens cured at room conditions and at higher temperature, were very satisfactory with good robustness and high average flexural strength (>2.5 MPa). The proposed mixture has a chance to be a viable space building material solution with enhanced composition or processing conditions. The results of this study showed that the properties of the mixture can be improved by either increasing temperature, hence speeding up the reaction, or increasing pressure, thus slowing down the water boiling out. Other improvements to the mixture can be increasing the alkalinity of the solution, which significantly speeds up the reaction, and is typically done by adding a strong hydroxide to the binder solution. Exploring potential mixture modifications and performing improved tests using the basis laid in this research might lead to a potentially effective and realistic way of utilizing Martian regolith for unmanned 3D-printing purposes with minimal investment, which is one of necessary goals in making a manned Martian mission possible.

References

1. Spudis, P.D., *Robots vs. Humans: Who Should Explore Space?-Astronaut explorers can perform science in space that robots cannot. Humans are needed to study planets and moons in detail and to repair scientific.* Scientific American, 1999(1): p. 24-31.
2. Bettiol, L., A. De La Torre, D. Patel, F. Oluwafemi, G. Kamaletdinova, R. Kumar Singh, U. Heshani, Y. Lakmal, A. Rivolta, and A. Sorokin. *Manned Mars Mission Risks Evaluation.* in *69th International Astronautical Congress (IAC 2018).* 2018.

3. Cucinotta, F.A., S. Hu, N.A. Schwadron, K. Kozarev, L.W. Townsend, and M.H.Y. Kim, *Space radiation risk limits and Earth-Moon-Mars environmental models.* Space Weather, 2010. **8**(12).
4. Missions, L.-D.E., *A Study on the Survivability and Adaptation of Humans to Long-Duration Exploratory Missions.* 2003.
5. Blüm, V., J. Gitelson, G. Horneck, and K. Kreuzberg, *Opportunities and constraints of closed man-made ecological systems on the moon.* Advances in Space Research, 1994. **14**(6): p. 271-280.
6. Kading, B. and J. Straub, *Utilizing in-situ resources and 3D printing structures for a manned Mars mission.* Acta Astronautica, 2015. **107**: p. 317-326.
7. Gannor, M.G., *News,"3D Printer Could Transform Moon Dirt Into Lunar Base.".* Space. com, 2015.
8. Ceccanti, F., E. Dini, X. De Kestelier, V. Colla, and L. Pambaguian. *3D printing technology for a moon outpost exploiting lunar soil.* in *61st International Astronautical Congress, Prague, CZ, IAC-10-D3.* 2010.
9. Soltani, A., R. Noroozi, M. Bodaghi, A. Zolfagharian, and R. Hedayati, *3D printing on-water sports boards with bio-inspired core designs.* Polymers, 2020. **12**(1): p. 250.
10. Ghavidelnia, N., M. Bodaghi, and R. Hedayati, *Idealized 3D auxetic mechanical metamaterial: an analytical, numerical, and experimental study.* Materials, 2021. **14**(4): p. 993.
11. Raval, S. *Exploration colonization resource extraction and utilization of Moon and Mars (ECROMM).* in *Proceedings of the 62nd International Astronautical Congress IAC.* 2011.
12. Hedayati, R., M. Mirzaali, L. Vergani, and A. Zadpoor, *Action-at-a-distance metamaterials: Distributed local actuation through far-field global forces.* APL Materials, 2018. **6**(3): p. 036101.
13. Hedayati, R., H. Hosseini-Toudeshky, M. Sadighi, M. Mohammadi-Aghdam, and A. Zadpoor, *Multiscale modeling of fatigue crack propagation in additively manufactured porous biomaterials.* International Journal of Fatigue, 2018. **113**: p. 416-427.
14. Hedayati, R., S.J. Salami, Y. Li, M. Sadighi, and A. Zadpoor, *Semianalytical geometry-property relationships for some generalized classes of pentamodelike additively manufactured mechanical metamaterials.* Physical Review Applied, 2019. **11**(3): p. 034057.
15. Ghavidelnia, N., M. Bodaghi, and R. Hedayati, *Femur Auxetic Meta-Implants with Tuned Micromotion Distribution.* Materials, 2021. **14**(1): p. 114.
16. Mohammadi, K., M. Movahhedy, I. Shishkovsky, and R. Hedayati, *Hybrid anisotropic pentamode mechanical metamaterial produced by additive manufacturing technique* Applied Physics Letters, 2020. **117**(6): p. 061901.
17. Jarrah, H.R., A. Zolfagharian, R. Hedayati, A. Serjouei, and M. Bodaghi. *Nonlinear finite element modelling of thermo-visco-plastic styrene and polyurethane shape memory polymer foams.* in *Actuators.* 2021. Multidisciplinary Digital Publishing Institute.
18. JeongAhn, Y. and R. Malhotra, *The current impact flux on Mars and its seasonal variation.* Icarus, 2015. **262**: p. 140-153.
19. Bland, P., T. Smith, A.T. Jull, F. Berry, A. Bevan, S. Cloudt, and C. Pillinger, *The flux of meteorites to the Earth over the last 50 000 years.* Monthly Notices of the Royal Astronomical Society, 1996. **283**(2): p. 551-565.
20. Toutanji, H., B. Glenn-Loper, and B. Schrayshuen. *Strength and durability performance of waterless lunar concrete.* in *43rd AIAA Aerospace Sciences Meeting and Exhibit.* 2005.
21. Lin, T., J.A. Senseney, L.D. Arp, and C. Lindbergh, *Concrete lunar base investigation.* Journal of Aerospace Engineering, 1989. **2**(1): p. 10-19.

22. Montes, C., K. Broussard, M. Gongre, N. Simicevic, J. Mejia, J. Tham, E. Allouche, and G.J.A.i.S.R. Davis, *Evaluation of lunar regolith geopolymer binder as a radioactive shielding material for space exploration applications.* 2015. **56**(6): p. 1212-1221.
23. Kim, M., S. Thibeault, J. Wilson, L. Heilbronn, R. Kiefer, J. Weakley, J. Dueber, T. Fogarty, and R. Wilkins, *Radiation protection using Martian surface materials in human exploration of Mars.* Physica Medica, 2001. **17**: p. 81-83.
24. Duxson, P., A. Fernández-Jiménez, J.L. Provis, G.C. Lukey, A. Palomo, and J.S. van Deventer, *Geopolymer technology: the current state of the art.* Journal of materials science, 2007. **42**(9): p. 2917-2933.
25. Davidovits, J., *Geopolymers: man-made rock geosynthesis and the resulting development of very early high strength cement.* Journal of Materials education, 1994. **16**: p. 91-91.
26. Puertas, F., B. González-Fonteboa, I. González-Taboada, M. Alonso, M. Torres-Carrasco, G. Rojo, and F. Martínez-Abella, *Alkali-activated slag concrete: Fresh and hardened behaviour.* Cement and Concrete Composites, 2018. **85**: p. 22-31.
27. Bakharev, T., J.G. Sanjayan, and Y.-B. Cheng, *Effect of elevated temperature curing on properties of alkali-activated slag concrete.* Cement and concrete research, 1999. **29**(10): p. 1619-1625.
28. Systems, T., *Tsr2000 series 3 axis dispensing robot - hardware instruction manual.* 2018.
29. Sagoe-Crentsil, K. and L. Weng, *Dissolution processes, hydrolysis and condensation reactions during geopolymer synthesis: Part II. High Si/Al ratio systems.* Journal of materials science, 2007. **42**(9): p. 3007-3014.
30. Hedayati, R., M. Sadighi, and M. Mohammadi-Aghdam, *On the difference of pressure readings from the numerical, experimental and theoretical results in different bird strike studies.* Aerospace Science and Technology, 2014. **32**(1): p. 260-266.
31. Hedayati, R. and S. Ziaei-Rad, *Foam-core effect on the integrity of tailplane leading edge during bird-strike event.* Journal of Aircraft, 2011. **48**(6): p. 2080-2089.
32. Hedayati, R. and S. Ziaei-Rad, *Effect of Impact Orientation on Bird Strike Analysis.* International Journal of Vehicle Structures & Systems (IJVSS), 2011. **3**(3).
33. Silnikov, M., I. Guk, A. Nechunaev, and N. Smirnov, *Numerical simulation of hypervelocity impact problem for spacecraft shielding elements.* Acta Astronautica, 2018. **150**: p. 56-62.
34. Calimanescu, I., N. Buzbuchi, and A. Dima, *Explicit dynamic simulation of a space debris projectile impact over a satellite structure.* J. Mar. Technol. Environ, 2009. **1**: p. 71-80.